THE JOURNAL OF BIOLOGICAL CHEMISTRY Vol. 278, No. 46, Issue of November 14, pp. 46081–46086, 2003
Printed in U.S.A.

Crystal Structure of the Human Natural Killer (NK) Cell Activating Receptor NKp46 Reveals Structural Relationship to Other Leukocyte Receptor Complex Immunoreceptors*

Received for publication, August 2, 2003
Published, JBC Papers in Press, September 4, 2003, DOI 10.1074/jbc.M308491200

Christine E. Foster‡, Marco Colonna§, and Peter D. Sun‡¶

From the ‡Structural Immunology Section, Laboratory of Immunogenetics, NIAID, National Institutes of Health, Rockville, Maryland 20852 and the §Department of Pathology and Immunology, Washington University School of Medicine, St. Louis, Missouri 63110

Natural cytotoxicity receptors (NCR) mediate lysis of a variety of tumor and virus-infected cells by natural killer (NK) cells. Upon engagement, NCR trigger the cytolytic activity and cytokine release of NK cells through association with ITAM-containing signaling molecules. To further understand the function of these receptors in activation of natural cytotoxicity, we determined the crystal structure of the extracellular ligand binding domain of human NKp46, one of three known NCR, at 2.2-Å resolution. The overall fold and disposition of the two C2-set immunoglobulin domains are similar to the D1D2 domains of inhibitory killer cell Ig-like receptor (KIR) and Ig-like transcript (ILT) receptors. As the cellular ligands of NKp46 have not yet been defined, the known ligand binding sites of KIR and ILT were compared with the corresponding structural regions of NKp46 in an effort to identify potential areas suitable for molecular recognition. A potential binding site for influenza hemagglutinin is located near the interdomain hinge, a region that mediates ligand binding in KIR. The structural similarity of NKp46 to inhibitory KIR receptors may have implications for how NK cells balance activating and inhibitory signals.

NK[1] cells contribute to the innate immune response by directly lysing certain autologous cells that have undergone tumor transformation or infection. NK cell-mediated cytotoxicity is modulated through the participation of two classes of cell surface receptors: activating receptors, which trigger the cytotoxic lysis of target cells, and inhibitory receptors, which transmit signals to block natural cytotoxicity. Inhibitory receptors, such as members of the KIR and murine Ly49 receptor families, primarily recognize class I major histocompatibility complex (MHC) molecules on target cells. Cells that have diminished or altered expression of class I MHC molecules, as may occur following viral infection or transformation, are unable to engage inhibitory receptors and become susceptible to lysis by NK cells (the "missing self" hypothesis) (1–3). The ligands of activation receptors are less well defined but also encompass class I MHC molecules and their homologs. For example, the stress-inducible MHC class I-related chains A and B and UL16 binding proteins are ligands of the activation receptor NKG2D (4, 5).

NK receptors that regulate natural cytotoxic functions belong to two structural classes, the Ig-like and the C-type lectin-like. Both classes have activating and inhibitory members. Despite this structural diversity, certain features unite receptors with common functions; inhibitory receptors contain cytoplasmic immunoreceptor tyrosine-based inhibitory motifs (ITIMs), through which they recruit specific Src homology 2-containing phosphatases following ligand engagement (6). Activating receptors, in contrast, have short cytoplasmic tails lacking tyrosine-based signaling motifs but contain a charged residue in their transmembrane domains through which they associate with activating motif-containing adapter proteins.

The natural cytotoxicity receptors (NCR) are a recently characterized family of Ig-like activation receptors that appear to be major triggering receptors in tumor cell recognition, although their ligands are not yet identified (7–13). To date, the three known NCR are NKp46 and NKp30, which are expressed by circulating NK cells, and NKp44, which is expressed only by activated NK cells (9, 11–14). NKp46 has been implicated in NK cell-mediated lysis of several autologous tumor and pathogen-infected cell lines, including melanoma, erythroleukemia, Epstein-Barr virus-transformed B cells, and *M. tuberculosis*-infected monocytes (9, 10, 13, 15). In antibody-mediated redirected lysis studies, NKp46 was shown to strongly activate NK cell functions including cytokine production and cytolytic activity, and blocking of NKp46 inhibited NK cell lysis of a series of class I MHC-negative target cells (9, 10, 13).

NKp46 has two Ig-like extracellular domains followed by a ~40-residue stalk region, a type I transmembrane domain, and a short cytoplasmic tail. Through a positively charged residue in the transmembrane region, the receptor associates with the ITAM-containing FcεRIγ and CD3ζ (12, 16). The gene encoding NKp46 is localized on the leukocyte Ig-like receptor complex on human chromosome 19, which contains a group of homologous immunoreceptors including the Ig-like transcripts (ILT), KIR, leukocyte-associated Ig-like receptors (LAIR), IgA Fc receptor

* This work was supported by intramural research funding of the NIAID, National Institutes of Health. The costs of publication of this article were defrayed in part by the payment of page charges. This article must therefore be hereby marked "*advertisement*" in accordance with 18 U.S.C. Section 1734 solely to indicate this fact.

The atomic coordinates and structure factors (code 1P6F) have been deposited in the Protein Data Bank, Research Collaboratory for Structural Bioinformatics, Rutgers University, New Brunswick, NJ (http://www.rcsb.org/).

¶ To whom correspondence should be addressed: Structural Immunology Section, Laboratory of Immunogenetics, NIAID, NIH, 12441 Parklawn Dr., Rockville, MD 20852. Tel.: 301-496-3230; Fax: 301-402-0284; E-mail: psun@niaid.nih.gov.

[1] The abbreviations used are: NK, natural killer; NCR, natural cytotoxicity receptor; MHC, major histocompatibility complex; ITIM, immunoreceptor tyrosine-based inhibitory motif; ITAM, immunoreceptor tyrosine-based activating motif; ILT, Ig-like transcript; KIR, killer cell Ig-like receptor; MIRAS, multiple isomorphous replacement with anomalous signaling; SMAC, supramolecular activation cluster; CTLR, C-type lectin-like receptor; PEG, polyethylene glycol; MOPS, 4-morpholinepropanesulfonic acid; HLA, human leukocyte antigen; TCR, T cell receptor.

(FcαRI), and platelet collagen receptor glycoprotein VI (17, 18). NKp46 genes have also been identified in other mammals, including cow, rat, and mouse (19–21). Despite common function, NKp46 has no significant homology to NKp30 and NKp44, which are encoded elsewhere in the genome. In efforts to understand the molecular basis of NCR-mediated NK cell activation, we determined the crystal structure of the extracellular ligand binding domains of human NKp46.

EXPERIMENTAL PROCEDURES

Protein Expression, Refolding, and Purification—The ectodomain of NKp46 (residues 1–235, excluding the signal sequence) was expressed in pET-22b with a C-terminal tag containing Leu-Glu followed by a His_6 purification tag. The receptor was expressed as inclusion bodies in BL21(DE3) cells and reconstituted by a dilution refolding procedure. In brief, inclusion bodies were redissolved in 8 M urea and rapidly diluted in a solution containing 0.1 M Tris-HCl, pH 8.0, 0.4 M arginine, 5 mM cysteamine, and 1 mM cystamine. The refolded protein was purified by immobilized metal affinity chromatography using nickel-nitrilotriacetic acid-agarose (Qiagen) followed by size exclusion chromatography on a Superdex 200 column (Amersham Biosciences).

Crystallization and Preparation of Heavy Atom Derivatives—NKp46 (9 mg/ml) was crystallized at 18 °C by hanging drop vapor diffusion over solutions containing 8–11% polyethylene glycol (PEG) 2000, 0.1 M MOPS at pH 7.2. Initial crystallization conditions were identified using microbatch procedures with an Oryx 6 robot crystallization station (Douglas Instruments). Crystals ($0.07 \times 0.07 \times 0.3$ mm) belong to space group $P6_1$ and contain one molecule per asymmetric unit. Heavy atom reagents were screened for reaction with NKp46 in solution by mass spectrometry (22). Mercury derivatives were generated using relatively high heavy atom reagent concentrations and shorter soak times (23, 24). Crystals Hg1 and Hg2 (Table I) were prepared by quick-soaking crystals in a solution containing 10 mM $HgCl_2$, 10–14% PEG 2000, 50 mM HEPES at pH 7.0 for 75–110 min. An additional mercury derivative (crystal Hg3) was prepared by soaking in a solution containing 10 mM $Hg(CH_3COO)_2$, 10% PEG 2000, 50 mM HEPES at pH 7.0 for 1 h. Lead-soaked crystals were prepared with longer soak times (4 h) in 16.7 mM $(CH_3)_3Pb(CH_3COO)_2$ (trimethyllead acetate), 10% PEG 4000, 50 mM MOPS at pH 7.2.

Data Collection and Processing—Prior to data collection, crystals were soaked in solutions containing glycerol (20–25%) for ~1 min and flash-frozen directly in a stream of liquid nitrogen. Native diffraction data were collected at Southeast Regional Collaborative Access Team (SER-CAT) 22-ID beamline at the Advanced Photon Source, Argonne National Laboratory. Supporting institutions may be found at www.ser.anl.gov/new/members.html. Derivative data were measured at beamline X9b at the National Synchrotron Light Source, Brookhaven National Laboratory. All data were integrated and scaled with HKL2000 (25).

Structure Solution and Refinement—Heavy atom sites were initially interpreted by SOLVE (26), and additional sites were located by difference Patterson techniques and refined using MLPHARE (27). The space group was confirmed by refinement of anomalous occupancies. MIRAS phases were initially calculated to 3.0 Å using data from three mercury- and one lead-derivatized crystals. Although the lead-soaked crystal was only weakly derivatized, its inclusion with the mercury derivatives appeared to improve the quality of the phases. Following solvent flattening and phase extension to 2.2 Å, the map was readily interpretable. Refinement of the structure against native data was carried out with CNS version 1.0 (28), and model building was performed using the program "O" (29). Residues in the CC′ loop of domain 2 were refined with lower occupancies due to weak electron density. Geometry of the refined structure was validated according to Ramachandran plot criteria of Lovell *et al.* (30). Analysis of interdomain hinge angles was performed with the program HINGE (31). Surface area calculations were made with CONTACT and AREAIMOL (27). Molecular figures were prepared with Molscript (32), Raster3D (33), GRASP (34), and Pymol (35). Potential glycosylation sites were identified by NetOGlyc and NetNGlyc (36).

RESULTS AND DISCUSSION

Overview of the Structure of NKp46 D1D2—The crystal structure of the extracellular ligand binding domain of NKp46 was determined to 2.2 Å by MIRAS phasing. Data collection and phasing statistics are listed in Table I. The refined structure includes residues 4–191, corresponding to the two N-terminal Ig domains. No interpretable electron density was found for the 40-residue stalk region that connects the two Ig domains to the transmembrane region. This suggests that the stalk is highly flexible and does not adopt a defined secondary structure. The two Ig domains of NKp46 are arranged in a V-shaped conformation, with an interdomain hinge angle of 85° (Fig. 1). Each Ig domain resembles that of a C2-set Ig fold, with two antiparallel β-sheets formed by strands *ABE* and *C′CFG*. NKp46 deviates from the canonical C2 Ig fold in that the first β-strand in each domain is interrupted by a cis proline and is split into two shorter strands A and A′, which pair with strands B and G, respectively. Additional short strands are formed between strands F and G; in D1 this short strand pairs with strand F, while in D2 it pairs with strand G of D1.

NKp46 contains short regions of helical conformation, including a 3_{10} helix in the EF loop of each domain. Residues preceding strand G adopt a polyproline II-type helical conformation, as observed in ILT2 (37). These residues overlap with sequence motifs similar to the WS*X*WS motifs first identified in hematopoietic receptors (37); in NKp46 these motifs are WS*XX*S and WSFPS in the N- and C-terminal domains, respectively. The side chains of the two serine residues within this motif are hydrogen bonded to main chain atoms in strand F, thus contributing to the stability of the core Ig fold.

The observed hinge angle of NKp46 (85°) is very similar to unliganded ILT2 (86°) and KIR2DL2 (84°) but is slightly larger than HLA-Cw3-bound KIR2DL2 (75°). Acute hinge angles are also common to Fc receptors such as FcγRIII and FcϵRI although their relative domain orientation is different (38, 39). The hinge angle of NKp46 is stabilized by both interdomain hydrogen bonds and hydrophobic interactions. Specifically, hydrogen bond pairings between the additional short strand of D2 and the G strand of D1 and between Arg^{145} and Asn^{175} and the presence of a salt bridge between Asp^{93} and His^{176} contribute to the hinge conformation. The hydrophobic hinge core is formed between residues from strands A′ and G in D1 and residues from strands C and C′, as well as the WSFPS motif in D2. The interface buries 1,021 $Å^2$ of accessible surface area, and comparison of NKp46 sequences across species reveals that 11 of 18 hinge core residues are conserved, indicating that the acute domain orientation is likely to be preserved.

Structural Comparison with Ig-like Immunoreceptors—The crystal structure of human NKp46 reported here can be contrasted with the structure of the NKp44 ectodomain, which is a single V-type Ig domain (40). In addition, a third disulfide bond observed in the structure of NKp44 is absent in NKp46. Furthermore, NKp30 is also predicted to contain a single V-type Ig domain.

The two-domain structure of NKp46 does resemble a number of Ig-like cell surface receptors. The closest structural relatives are other leukocyte receptor complex immunoreceptors, including KIR, ILT, and FcαRI (CD89), which are 31–35% identical to NKp46 at the protein sequence level. NKp46 also has structural similarity to FcγRIIb and other Fc receptors of known structure, although sequence identity to these is less than 20%. Structures of the D1D2 domains of three KIR family proteins have been determined alone and in complex with class I MHC ligands (31, 41–44). Superposition of NKp46 with KIR2DL2 (Fig. 2*A*) resulted in a root mean square (r.m.s.) deviation of 1.1 Å for 71 α-carbon atoms in D1 and 0.9 Å for 78 α-carbon atoms in D2. The D1D2 moieties of ILT2 (LIR-1) and ILT4 (LIR-2) (37, 45) are also closely related in structure to NKp46. Superposition of ILT2 with NKp46 (Fig. 2*B*) resulted in r.m.s. deviations of 0.9 Å (66 α-carbon atoms) and 1.4 Å (80 α-carbon atoms) for D1 and D2, respectively. The recently reported structures of the FcαRI ectodomain (46, 47) and its complex with Fcα (47)

TABLE I
Crystallographic data collection and refinement statistics

	Native	Hg1[a]	Hg2	Hg3	Pb
Wavelength (Å)	1.0093	0.9931	1.0093	0.9931	0.9392
Unit cell parameters (Å)	$a = b = 85.73$, $c = 59.52$	$a = b = 86.18$, $c = 59.34$	$a = b = 86.27$, $c = 59.03$	$a = b = 86.04$, $c = 59.22$	$a = b = 85.02$, $c = 59.21$
Resolution range (Å)	50–2.2	50–3.0	50–3.4	50–3.1	50–2.7
Total observations	347,922	61,642	27,449	46,321	85,580
Unique reflections	12,785	5,141	3,459	4,145	6,818
Completeness (%)	97.8 (83.3)[b]	99.8 (100.0)	90.9 (16.5)	95.0 (97.8)	99.5 (99.4)
$\langle I/\sigma(I)\rangle$	21.2 (2.2)	13.2 (2.2)	17.5 (4.8)	7.9 (1.7)	17.5 (3.0)
R_{sym} (%)[c]	7.1 (30.8)	13.8 (75.9)	5.5 (18.1)	10.5 (53.0)	6.2 (39.4)
Phasing statistics					
R_{iso} (%)[d]		0.281	0.268	0.274	0.117
Number of sites		3	3	3	3
Phasing power (acentric/centric)[e]		2.5/1.5	2.3/1.3	2.6/1.5	0.60/0.52
R_{cullis} (acentric/centric)[f]		0.56/0.69	0.60/0.74	0.56/0.65	0.91/0.87
Overall figure of merit (15–3 Å)	0.59				
Refinement statistics					
Resolution range (Å)	20–2.2				
R_{cryst} (%)[g]	20.6				
R_{free} (%)	25.0				
Mean *B*-factor (Å^2)	41.9				
Number of atoms					
Protein	1,500				
Water	87				
r.m.s. deviations from ideality					
Bond lengths (Å)	0.008				
Angles (°)	1.47				
Ramachandran plot, residues in:					
Most favored regions (%)	94.6				
Allowed regions (%)	100				

[a] The Hg1 and Hg2 crystals were soaked in $HgCl_2$ for 75 and 110 min, respectively; the Hg3 crystal was soaked in $Hg(CH_3COO)_2$ for 1 h, and the lead crystal was soaked in trimethyl lead acetate for 4 h.
[b] Values in parentheses are given for the highest resolution shell.
[c] $R_{sym} = \Sigma_{hkl}|I_{hkl} - \langle I_{hkl}\rangle|/\Sigma_{hkl}I_{hkl}$.
[d] $R_{iso} = \Sigma||F_{PH}| - |F_P||/\Sigma|F_P|$, where F_{PH} is the structure factor amplitude of the derivative crystal and F_P is that of the native crystal.
[e] Phasing power = (heavy atom amplitude)/(lack of closure error).
[f] R_{cullis} = (lack of closure error)/(isomorphous difference).
[g] $R = \Sigma|F_{obs} - F_{calc}|/\Sigma|F_{obs}|$. R_{cryst} and R_{free} were calculated from working and test sets of reflections, respectively; the test set was composed of 1,284 (10%) reflections that were excluded from refinement.

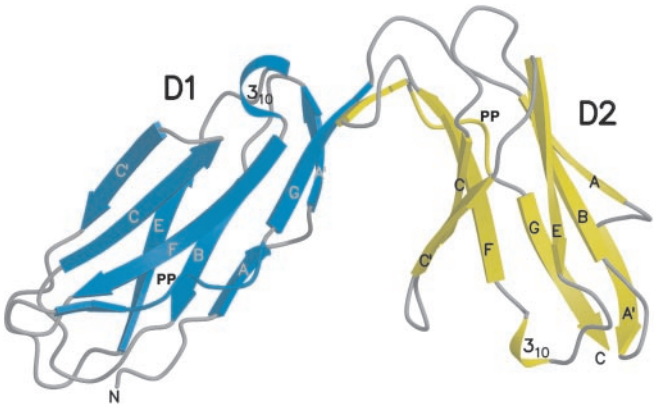

FIG. 1. **The crystal structure of NKp46 D1D2.** Shown are secondary structure elements of domains 1 (*blue*) and 2 (*yellow*), with regions of coil in gray. Helical regions, including polyproline II-type helices (*PP*), are labeled.

also underscore the structural relationship between leukocyte Ig-like receptor complex members. The structure of free FcαRI (47) was superimposed with NKp46 (Fig. 2*C*) with r.m.s. deviations of 2.1 Å (D1, 70 α-carbon atoms) and 1.9 Å (D2, 93 α-carbon atoms). NKp46 can be distinguished primarily from KIR, ILT, and FcαRI by the conformation and length of several loops. For example, the CC′ loop in D1 is shorter than in KIR, ILT2, and FcαRI. Like KIR and Fcα-complexed FcαRI, NKp46 contains a longer C′ strand in D1 as compared with ILT2 and free FcαRI, which are followed by a helical stretch and a D strand, respectively. The C′E loop in D1 has divergent conformations in the structures examined; in NKp46 this loop includes three proline residues and three basic residues and adopts an unusual meandering conformation. The nearby FG loop adopts similar conformations in NKp46 and FcαRI, while in ILT2 it is twisted relative to the plane of the FG strands and in KIR it is lengthened by three residues and forms a protruding flap (Fig. 2*A*). In D2, the C′E and FG loops vary in length among the receptors. The EF loop also varies, although the conformation in NKp46 resembles that in FcαRI, including a single turn of 3_{10} helix.

Implications for Ligand Binding—NKp46 has been reported to bind both influenza virus hemagglutinin and Sendai virus hemagglutinin-neuraminidase, and this interaction appears to involve terminal sialic residues on NKp46 (48). Human NKp46 is predicted to contain a single *N*-linked (Asn^{195}) and two *O*-linked (Thr^{104} and Thr^{204}) glycosylation sites. Two of these sites (Asn^{195} and Thr^{204}) are located in the membrane proximal stalk, which was disordered in the structure. Thr^{104} is located in D1D2 in a solvent-exposed position near the D1-D2 juncture. This location is close to the ligand binding site of KIR receptors (see below). However, none of the three putative glycosylation sites in human NKp46 are conserved in all species.

To date, no cellular ligands of NKp46 have been identified, although NKp46 has been shown to mediate NK cell cytolysis of certain human tumor cells. A murine homolog of NKp46 has been identified (20), which is 58% identical to the human receptor (Fig. 3). Intriguingly, it has been reported that murine tumor cells are susceptible to killing via human NKp46 (9, 10). This cross-species killing may suggest a conserved ligand binding site shared between the human and mouse receptors. A similar case exists between human and murine NKG2D receptors; although murine NKG2D, which is capable of recognizing

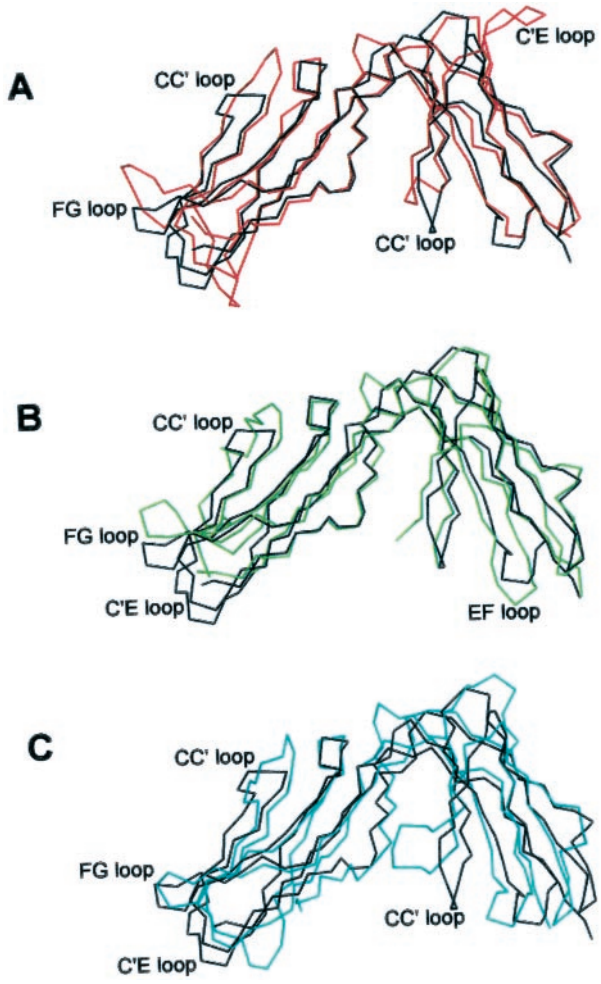

FIG. 2. **Comparison of NKp46 to other Ig-like receptors.** The structure of NKp46 (*black*) is superimposed with that of KIR2DL2 (*red*) in *A*, with ILT2 (*green*) in *B*, and with FcαRI (*aqua*) in *C*.

human ULBP molecules, shares 60% overall sequence identity with its human counterpart, nearly all ligand binding residues are conserved. To evaluate potential ligand binding sites, we examined the sequence conservation of two structural regions on NKp46 that correspond to the known ligand binding sites of the homologous KIR and ILT receptors.

The first region corresponds to the HLA binding site on KIR receptors. KIR2DL2 uses six surface loops at the interdomain hinge region to recognize the α1-α2 peptide binding region of HLA-C molecules (41, 43). This site appears to be electrostatic in nature and is relatively flat, with many ligand contacting residues positioned in a platform-like plane (Fig. 4*A*). In comparison, NKp46 has a less prominent platform than KIR due to two slightly shorter surface loops, the CC′ loop of D1 and the FG loop of D2 (Fig. 4*C*). Moreover, the electrostatic surface of NKp46 is less markedly charged than KIR in this area (Fig. 5), suggesting that ligand recognition via this surface would be less dominated by electrostatic interactions than KIR-MHC recognition. This region encompasses ~1,400 Å^2 of accessible surface area and includes the conserved residues Ser^{69}, Tyr^{100}, Asp^{101}, Thr^{102}, Thr^{127}, Thr^{129}, Ser^{130}, Tyr^{173}, Asn^{174}, Ala^{177}, and Phe^{180}.

A second putative ligand binding site is delineated by FcαRI binding to Fcα, which involves residues from strand C′ and from the BC, C′E, and FG loops on the N-terminal domain of the receptor (47, 49, 50). In addition, the UL18 binding site on ILT2 has been mapped by mutagenesis and appears to overlap with the FcαRI ligand binding region (37, 51). The FcαRI surface includes hydrophobic contacts and surrounding basic residues (Fig. 5*D*). Comparison of the structure of this region with NKp46 reveals that the most apparent difference is in the conformation of the C′E looop, which is two residues shorter in FcαRI and is shifted ~4 Å. In NKp46 this loop appears to be constrained by the presence of three proline residues: Pro^{51}, Pro^{53}, and Pro^{54}. Like FcαRI, however, NKp46 also contains a number of basic residues in this area, including Arg^{50}, Lys^{52}, and Arg^{56} in the C′E loop and Arg^{80} in the FG loop. Several solvent-exposed residues within the BC, C′E, and FG loops of NKp46 were selected as possible components of an FcαRI-like binding site (Fig. 4*D*). With inclusion of the predicted ILT2 ligand binding site, this surface covers ~1,300 Å^2 of accessible surface area. Like the KIR-like binding site, this region also features clusters of conserved residues. Of 17 residues located in this putative FcαRI/ILT2-like binding site, those conserved among NKp46 sequences are Glu^{36} and Gln^{38} (C strand), Arg^{50}, Pro^{51}, and Lys^{52} (C′E loop), Tyr^{78} (F strand), and Gly^{82} and Glu^{83} (FG loop).

The structural similarity of NKp46 to related immunoreceptors encoded within the human leukocyte receptor complex has raised the possibility that similar receptor surfaces are employed in ligand recognition. We examined two potential ligand binding sites on the structure of NKp46 that correspond to those employed by KIR and FcαRI/ILT2. The region analogous to the KIR ligand binding site is located at the interdomain hinge and involves residues from both domains; the loop structure of this surface largely resembles that of KIR. In comparison, the putative FcαRI-like site on the membrane distal domain covers a similar surface area, but the loop structure in this area is more divergent in NKp46. Although the close structural relationship between these receptors suggests that these two sites are the most likely candidates for ligand recognition in NKp46, the plasticity of the Ig fold is manifested in the use of different binding surfaces by FcαRI and KIR, and it is possible that NKp46 interacts with ligand using a distinct site. It is clear that elucidation of the activation mechanisms of NKp46 and other natural cytotoxicity receptors will require further studies to identify their ligands on target cells and to define the molecular recognition between these receptors and their ligands.

Implications for the Structure and Function of the NK Immune Synapse—The structural resemblance between the activating receptor NKp46 and inhibitory KIR receptors may have implications regarding the function of NK cells. Similar to T cells, the signaling of NK cells occurs in a synaptic structure at the site of contact between NK and target cells. Although the structure of the NK cell immune synapse has not been well defined, regions similar to the supramolecular activation clusters (SMACs) observed in T cell immune synapses were also observed in NK cell immune synapses (52). In the case of T cell signaling, it is known that different receptors cluster preferentially in different SMACs and that each SMAC region contains a dynamically regulated heterogeneous population of receptors (53). For example, CD8, TCR, and protein kinase C θ were found in the cSMAC, whereas LFA-1 and talin were found in the pSMAC of the CD8 T cell immune synapse (54). It has been postulated that the local shape and spacing of the membrane, which depend on the size of surface receptors, dictate the receptor clustering at the point of cell-cell contact (55). This is likely to be true in the absence of strong homotypic receptor-receptor interactions. Unlike individual T cells, which possess only TCR as their activation receptor, individual NK cells express multiple forms of activating and inhibitory receptors. An obvious question is whether the NK immune synapse contains primarily a cluster of homogeneous receptors or multiple forms

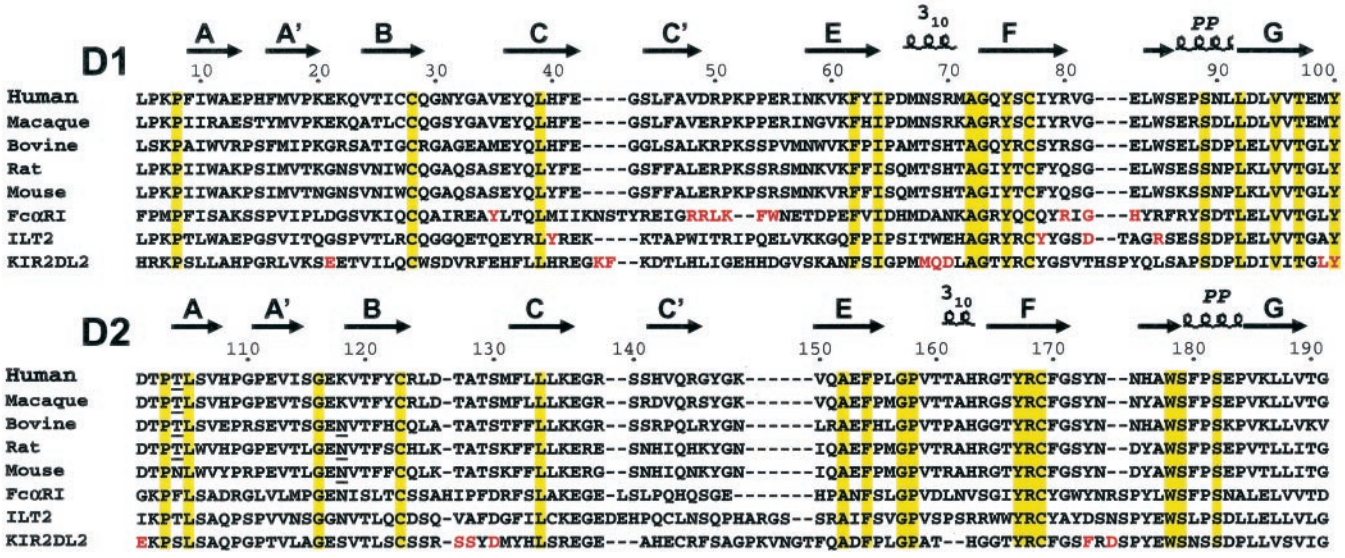

FIG. 3. **Alignment of NKp46 D1D2 sequences and related proteins.** Secondary structure elements of human NKp46 are shown above sequences. *Arrows* indicate β-strands, *coils* indicate helices, and "*PP*" indicates polyproline II-type helices. Conserved residues are highlighted in *yellow*. For NKp46 sequences, putative glycosylation sites are *underlined*. Residues implicated in ligand binding are in *red*. Accession codes for sequences are: human NKp46, AJ001383; macaque NKp46, AJ278288; bovine NKp46, AAP33623; rat NKp46, NM_057199; mouse NKp46, NM_010746; KIR2DL2, P43627; ILT2, AAC51179; FcαRI, BAB64914.

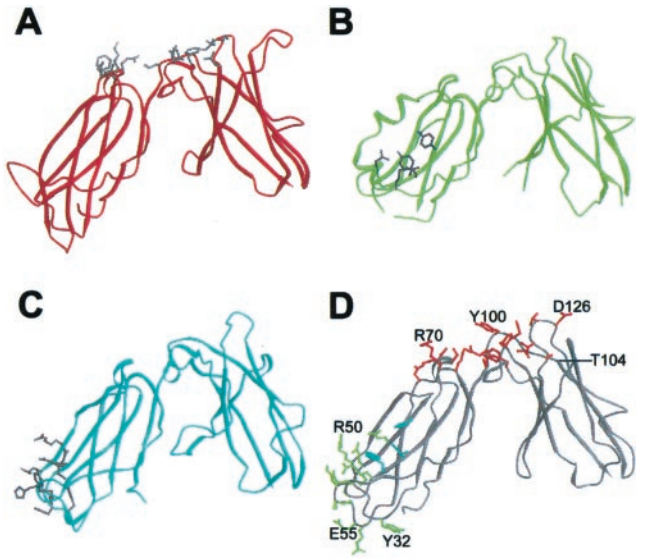

FIG. 4. **Ligand binding sites of leukocyte receptor complex immunoreceptors.** *A*, the structure of KIR2DL2 (Protein Data Bank entry 1efx) with residues contacting HLA-Cw3 displayed as *ball-and-stick* models in *gray* (41). *B*, ILT2 (1g0x) with residues implicated in binding to UL18 (37, 51). *C*, FcαRI (10W0) with residues contacting Fcα displayed. *D*, the structure of NKp46 with putative ligand binding residues displayed. Residues in *red* correspond to the KIR binding site; those in *aqua* and *green* correspond to the FcαRI and ILT2 binding sites, respectively. The location of the potentially glycosylated residue Thr^{104} is shown.

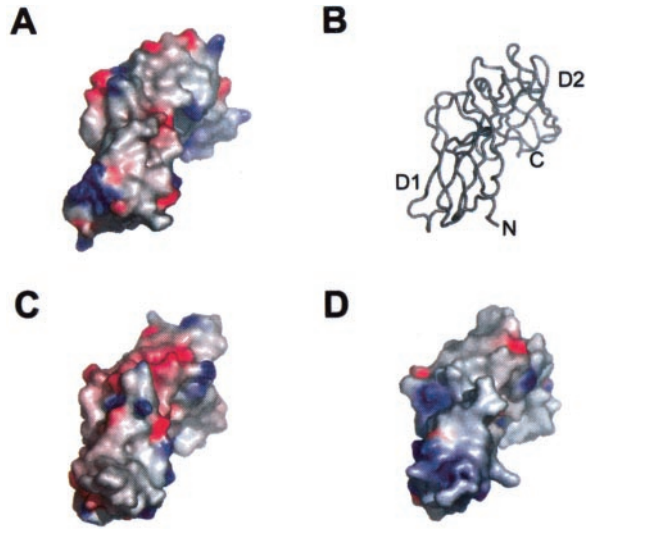

FIG. 5. **Surface representation of NKp46 and related receptors.** Shown are the molecular surfaces of NKp46 (*A*), KIR2DL2 (C), and FcαRI (*D*) colored by electrostatic potential. The α-carbon trace of NKp46 is shown in *B* for orientation.

of heterogeneous receptors. The structural resemblance between NKp46 and the inhibitory KIR2D receptors, as well as between the highly homologous inhibitory and non-inhibitory KIRs, suggests that both activating and inhibitory receptors could coexist in the NK immune synapse. It is tempting to speculate that the structural homology between NKp46, KIR2DS, and KIR2DL may lead to colocalization of all three receptors in a single synaptic structure. Such a heterogeneous receptor clustering would bring DAP12 and inhibitory ITIMs into close proximity and predicts that the outcome of NK cell activation depends upon the balance between the activating and inhibitory forms of the receptors. In fact, the structurally homologous activating and inhibitory receptor pairs are also observed between the C-type lectin-like receptors (CTLR), such as between the inhibitory CD94/NKG2A, and the activating CD94/NKG2C and NKG2D receptors. By the same argument, it is possible that a cluster of CTLR receptors may contain both activating and inhibitory forms. The observed dominance of the inhibitory signals could be due to either their higher ligand affinity or their surface abundance compared with the activating receptors. Recently, NCRs were shown to "cross-talk" among their associated signaling molecules (56), suggesting the possibility of colocalization of structurally diverse NCRs in an NK immune synapse. Indeed, a survey of the known NK receptor structures, including NCR, KIR, CD94/NKG2, and NKG2D, reveals that the dimensions of their ligand binding domains, excluding the flexible membrane proximal stalk region, range between 40 and 60 Å. This is in contrast with the dimensions of integrin molecules, which span ~250 Å. It is thus possible that all signaling NK receptors reside in a common

region distinct from that of LFA-1 in the NK immune synapse and that the net outcome of NK cell activation upon engagement of a target cell depends on the overall balance of all forms of receptors conjugated at the cell-cell contact.

Acknowledgments—We thank C. Hammer for performing mass spectrometry determinations; B. Hagos for assistance with protein expression; and S. Radaev, A. Johnson, Z. Dauter, J. Chrzas, and N. Leyarovska for assistance with synchrotron data collection. S. Radaev also provided helpful comments on the manuscript. Use of the Advanced Photon Source was supported by the United States Department of Energy, Basic Energy Sciences, Office of Science, under Contract No. W-31-109-Eng-38.

Addendum—After submission of this manuscript, the crystal structure of ILT2 (LIR-1) in complex with HLA-A2 was reported by Wilcox *et al*. (57). This work revealed that ILT2 recognizes HLA-A2 not only via residues in domain 1 (in agreement with prior mutagenesis studies) but also via residues at the interdomain hinge.

REFERENCES

1. Karre, K., Ljunggren, H. G., Piontek, G., and Kiessling, R. (1986) *Nature* **319,** 675–678
2. Karre, K. (2002) *Scand. J. Immunol.* **55,** 221–228
3. Ljunggren, H. G., and Karre, K. (1985) *J. Exp. Med.* **162,** 1745–1759
4. Bauer, S., Groh, V., Wu, J., Steinle, A., Phillips, J. H., Lanier, L. L., and Spies, T. (1999) *Science* **285,** 727–729
5. Cosman, D., Mullberg, J., Sutherland, C. L., Chin, W., Armitage, R., Fanslow, W., Kubin, M., and Chalupny, N. J. (2001) *Immunity* **14,** 123–133
6. Lanier, L. L. (1998) *Annu. Rev. Immunol.* **16,** 359–393
7. Moretta, A., Biassoni, R., Bottino, C., Mingari, M. C., and Moretta, L. (2000) *Immunol. Today* **21,** 228–234
8. Moretta, A., Bottino, C., Vitale, M., Pende, D., Cantoni, C., Mingari, M. C., Biassoni, R., and Moretta, L. (2001) *Annu. Rev. Immunol.* **19,** 197–223
9. Pessino, A., Sivori, S., Bottino, C., Malaspina, A., Morelli, L., Moretta, L., Biassoni, R., and Moretta, A. (1998) *J. Exp. Med.* **188,** 953–960
10. Sivori, S., Pende, D., Bottino, C., Marcenaro, E., Pessino, A., Biassoni, R., Moretta, L., and Moretta, A. (1999) *Eur. J. Immunol.* **29,** 1656–1666
11. Pende, D., Parolini, S., Pessino, A., Sivori, S., Augugliaro, R., Morelli, L., Marcenaro, E., Accame, L., Malaspina, A., Biassoni, R., Bottino, C., Moretta, L., and Moretta, A. (1999) *J. Exp. Med.* **190,** 1505–1516
12. Vitale, M., Bottino, C., Sivori, S., Sanseverino, L., Castriconi, R., Marcenaro, E., Augugliaro, R., Moretta, L., and Moretta, A. (1998) *J. Exp. Med.* **187,** 2065–2072
13. Sivori, S., Vitale, M., Morelli, L., Sanseverino, L., Augugliaro, R., Bottino, C., Moretta, L., and Moretta, A. (1997) *J. Exp. Med.* **186,** 1129–1136
14. Cantoni, C., Bottino, C., Vitale, M., Pessino, A., Augugliaro, R., Malaspina, A., Parolini, S., Moretta, L., Moretta, A., and Biassoni, R. (1999) *J. Exp. Med.* **189,** 787–796
15. Vankayalapati, R., Wizel, B., Weis, S. E., Safi, H., Lakey, D. L., Mandelboim, O., Samten, B., Porgador, A., and Barnes, P. F. (2002) *J. Immunol.* **168,** 3451–3457
16. Moretta, A., Bottino, C., Millo, R., and Biassoni, R. (1999) *Curr. Top. Microbiol. Immunol.* **244,** 69–84
17. Martin, A. M., Kulski, J. K., Witt, C., Pontarotti, P., and Christiansen, F. T. (2002) *Trends Immunol.* **23,** 81–88
18. Wagtmann, N., Rojo, S., Eichler, E., Mohrenweiser, H., and Long, E. O. (1997) *Curr. Biol.* **7,** 615–618
19. Storset, A. K., Slettedal, I. O., Williams, J. L., Law, A., and Dissen, E. (2003) *Eur. J. Immunol.* **33,** 980–990
20. Biassoni, R., Pessino, A., Bottino, C., Pende, D., Moretta, L., and Moretta, A. (1999) *Eur. J. Immunol.* **29,** 1014–1020
21. Falco, M., Cantoni, C., Bottino, C., Moretta, A., and Biassoni, R. (1999) *Immunol. Lett.* **68,** 411–414
22. Sun, P. D., and Hammer, C. H. (2000) *Acta Crystallogr. Sect. D Biol. Crystallogr.* **56,** 161–168
23. Sun, P. D., and Radaev, S. (2002) *Acta Crystallogr. Sect. D Biol. Crystallogr.* **58,** 1099–1103
24. Sun, P. D., Radaev, S., and Kattah, M. (2002) *Acta Crystallogr. Sect. D Biol. Crystallogr.* **58,** 1092–1098
25. Otwinowski, Z., and Minor, W. (1997) *Methods Enzymol.* **276,** 307–326
26. Terwilliger, T. C., and Berendzen, J. (1999) *Acta Crystallogr. Sect. D Biol. Crystallogr.* **55,** 849–861
27. Collaborative Computational Project Number 4 (1994) *Acta Crystallogr. Sect. D Biol. Crystallogr.* **50,** 760–763
28. Brunger, A. T., Adams, P. D., Clore, G. M., DeLano, W. L., Gros, P., Grosse-Kunstleve, R. W., Jiang, J. S., Kuszewski, J., Nilges, M., Pannu, N. S., Read, R. J., Rice, L. M., Simonson, T., and Warren, G. L. (1998) *Acta Crystallogr. Sect. D Biol. Crystallogr.* **54,** 905–921
29. Jones, T. A., Zou, J.-Y., Cowan, S. W., and Kjeldgaard, M. (1991) *Acta Crystallogr. Sect. A* **47,** 110–119
30. Lovell, S. C., Davis, I. W., Arendall, W. B., III, de Bakker, P. I., Word, J. M., Prisant, M. G., Richardson, J. S., and Richardson, D. C. (2003) *Proteins* **50,** 437–450
31. Snyder, G. A., Brooks, A. G., and Sun, P. D. (1999) *Proc. Natl. Acad. Sci. U. S. A.* **96,** 3864–3869
32. Kraulis, P. J. (1991) *J. Appl. Crystallogr.* **24,** 946–950
33. Merritt, E. A., and Bacon, D. J. (1997) *Methods Enzymol.* **277,** 505–524
34. Nicholls, A., Sharp, K. A., and Honig, B. (1991) *Proteins* **11,** 281–296
35. DeLano, W. L. (2002) *The PyMOL Molecular Graphics System*, DeLano Scientific, San Carlos, CA
36. Hansen, J. E., Lund, O., Tolstrup, N., Gooley, A. A., Williams, K. L., and Brunak, S. (1998) *Glycoconj. J.* **15,** 115–130
37. Chapman, T. L., Heikema, A. P., West, A. P., Jr., and Bjorkman, P. J. (2000) *Immunity* **13,** 727–736
38. Garman, S. C., Kinet, J. P., and Jardetzky, T. S. (1999) *Annu. Rev. Immunol.* **17,** 973–976
39. Zhang, Y., Boesen, C. C., Radaev, S., Brooks, A. G., Fridman, W. H., Sautes-Fridman, C., and Sun, P. D. (2000) *Immunity* **13,** 387–395
40. Cantoni, C., Ponassi, M., Biassoni, R., Conte, R., Spallarossa, A., Moretta, A., Moretta, L., Bolognesi, M., and Bordo, D. (2003) *Structure* (*Camb.*) **11,** 725–734
41. Boyington, J. C., Motyka, S. A., Schuck, P., Brooks, A. G., and Sun, P. D. (2000) *Nature* **405,** 537–543
42. Fan, Q. R., Mosyak, L., Winter, C. C., Wagtmann, N., Long, E. O., and Wiley, D. C. (1997) *Nature* **389,** 96–100
43. Fan, Q. R., Long, E. O., and Wiley, D. C. (2001) *Nat. Immunol.* **2,** 452–460
44. Maenaka, K., Juji, T., Stuart, D. I., and Jones, E. Y. (1999) *Struct. Fold. Des.* **7,** 391–398
45. Willcox, B. E., Thomas, L. M., Chapman, T. L., Heikema, A. P., West, A. P., Jr., and Bjorkman, P. J. (2002) *BMC Structure Biology* http://biomedcentral.com/1472-6807/2/6
46. Ding, Y., Xu, G., Yang, M., Yao, M., Gao, G. F., Wang, L., Zhang, W., and Rao, Z. (2003) *J. Biol. Chem.* **278,** 27966–27970
47. Herr, A. B., Ballister, E. R., and Bjorkman, P. J. (2003) *Nature* **423,** 614–620
48. Mandelboim, O., Lieberman, N., Lev, M., Paul, L., Arnon, T. I., Bushkin, Y., Davis, D. M., Strominger, J. L., Yewdell, J. W., and Porgador, A. (2001) *Nature* **409,** 1055–1060
49. Wines, B. D., Hulett, M. D., Jamieson, G. P., Trist, H. M., Spratt, J. M., and Hogarth, P. M. (1999) *J. Immunol.* **162,** 2146–2153
50. Wines, B. D., Sardjono, C. T., Trist, H. H., Lay, C. S., and Hogarth, P. M. (2001) *J. Immunol.* **166,** 1781–1789
51. Chapman, T. L., Heikeman, A. P., and Bjorkman, P. J. (1999) *Immunity* **11,** 603–613
52. Davis, D. M., Chiu, I., Fassett, M., Cohen, G. B., Mandelboim, O., and Strominger, J. L. (1999) *Proc. Natl. Acad. Sci. U. S. A.* **96,** 15062–15067
53. Freiberg, B. A., Kupfer, H., Maslanik, W., Delli, J., Kappler, J., Zaller, D. M., and Kupfer, A. (2002) *Nat. Immunol.* **3,** 911–917
54. Potter, T. A., Grebe, K., Freiberg, B., and Kupfer, A. (2001) *Proc. Natl. Acad. Sci. U. S. A.* **98,** 12624–12629
55. Dustin, M. L. (2002) *Arthritis Res.* **4,** Suppl. 3, S119–S125
56. Augugliaro, R., Parolini, S., Castriconi, R., Marcenaro, E., Cantoni, C., Nanni, M., Moretta, L., Moretta, A., and Bottino, C. (2003) *Eur. J. Immunol.* **33,** 1235–1241
57. Wilcox, B. E., Thomas, L. M., and Bjorkman, P. J. (2003) *Nat. Immunol.* **4,** 913–919